AIAA 2004-0822

Thermal Resistances of Gaseous Gap for Non-Conforming Rough Contacts

M. Bahrami, J. R. Culham and M. M. Yovanovich
Microelectronics Heat Transfer Laboratory
Department of Mechanical Engineering, University of Waterloo
Waterloo, Ontario, Canada N2L 3G1

42nd AIAA Aerospaces Meeting and Exhibit
Jan 5-8, 2004/Reno, Nevada

Thermal Resistances of Gaseous Gap for Non-Conforming Rough Contacts

M. Bahrami*, J. R. Culham† and M. M. Yovanovich‡
Microelectronics Heat Transfer Laboratory
Department of Mechanical Engineering, University of Waterloo
Waterloo, Ontario, Canada N2L 3G1

An approximate analytical model is developed for predicting the thermal contact resistance of spherical rough solids with the presence of interstitial gases. The joint resistance includes four thermal resistances, i.e., macrogap, microgap, macrocontact, and microcontacts. Simple relationships are derived for each component of the joint resistance assuming contacting surfaces are of uniform temperature and that the microgap heat transfer area and the macrocontact area are identical. Effects of main input contact parameters on the joint resistance are studied. It is demonstrated that a surface curvature exists that minimizes the joint resistance for a fixed contact. The model covers all regimes of gas heat conduction modes from continuum to free molecular. The present model is compared with 110 experimental data points collected by Kitscha and good agreement is shown over entire range of the comparison.

Nomenclature

A	=	area, m^2
a	=	radius of contact, m
b_L	=	specimens radius, m
c_1	=	Vickers microhardness coefficient, Pa
c_2	=	Vickers microhardness coefficient
d	=	mean contacting bodies distance, m
E	=	Young's modulus, Pa
E'	=	equivalent elastic modulus, Pa
F	=	external force, N
H'	=	$c_1 \left(1.62\sigma'/m\right)^{c_2}$, Pa
Kn	=	Knudsen number
k	=	thermal conductivity, W/mK
m	=	mean absolute surface slope
M	=	gas parameter, m
P	=	pressure, Pa
Pr	=	Prandtl number
Q	=	heat flow rate, W
q	=	heat flux, W/m^2
R	=	thermal resistance, K/W
r, z	=	cylindrical coordinates
T	=	temperature, K
TAC	=	thermal accomodation coefficient
TCR	=	thermal contact resistance
vac	=	vacuum
Y	=	mean surface plane separation, m

Greek

α	=	non-dimensional parameter, $\equiv \sigma\rho/a_H^2$
γ	=	exponent of the general pressure distribution
γ_g	=	ratio of gas specific heats
Λ	=	mean free path, m
δ	=	maximum surface out-of-flatness, m
λ	=	non-dimensional separation$\equiv Y/\sqrt{2}\sigma$
ν	=	Poisson's ratio
ξ	=	non-dimensional radial position, $\equiv r/a_L$
ρ	=	radius of curvature, m
σ	=	RMS surface roughness, m
σ'	=	σ/σ_0, $\sigma_0 = 1\ \mu m$
τ	=	non-dimensional parameter, $\equiv \rho/a_H$
ω	=	bulk normal deformation, m

Subscripts

0	=	reference value
1, 2	=	solid 1, 2
a	=	apparent
g	=	gas, microgap
G	=	macrogap
H	=	Hertz
L	=	macrocontact
j	=	joint
r	=	real
s	=	solid, micro

Introduction

A surface is characterized not only by the roughness but also by its curvature/out-of-flatness. When non-conforming random rough surfaces are placed in mechanical contact, due to the surface roughness *real* contacts or microcontacts occur at the top of surface asperities. As a result of surface out-of-flatness or curvature, the microcontacts are distributed in the macrocontact area, A_a. In addition, the contact pressure is not uniform and it asymptotically approaches zero at the edge of the macrocontact area, $r = a_L$. The real contact area, A_r, the summation of microcontacts is typically a small fraction of the nominal

*Ph.D. Candidate, Department of Mechanical Engineering.
†Associate Professor, Director, Microelectronics Heat Transfer Laboratory.
‡Distinguished Professor Emeritus, Department of Mechanical Engineering. Fellow AIAA.

contact area.

Geometry of non-conforming rough contacts is shown in Fig. 1, where two cylindrical solids with the radius of b_L are pressed against each other with external load, F. The gap between contacting bodies is filled with an interstitial gas at pressure P_g and heat is being transferred from one body to another. Generally, heat transfer through the contact interface is not limited to conduction through the actual contact area. Rather, heat transfer across a solid joint can occur via three distinct modes, radiative transfer, conduction through interstitial material in the gap, and conduction through the real contact area. As mentioned in part one of this study,[1] thermal radiation across the gap in most applications can be neglected, thus the remaining heat transfer modes are conduction through the microcontacts and conduction through the interstitial gas filled the gap between contacting bodies. As shown in Fig. 1, heat transfer occurs through three main paths, interstitial gas within the microgap Q_g, microcontacts Q_s, and interstitial gas within the macrogap, Q_G. As a result of the small real contact area and low thermal conductivities of interstitial gases, heat flow experiences a relatively large thermal resistance passing through the joint, this phenomenon leads to a relatively high temperature drop across the interface.

The rate of heat transfer across the non-conforming rough joints depends on a number of parameters: thermal properties of solids and gas, elastic and plastic mechanical properties of solids, gas pressure, surface curvature or out-of-flatness, surface roughness characteristics, and applied load.

In applications where the contact pressure is relatively low, the real contact area is limited to an even smaller portion of the apparent area, i.e., $A_r \sim 0.01A_a$. Consequently, the heat transfer takes place mainly through the interstitial gas in the gap. The relative magnitude of the gap heat transfer varies greatly with the size of the macrocontact, applied load, surface roughness, gas pressure and thermal conductivities of the gas and solids. As the contact pressure increases, the heat transfer through the microcontacts increases and becomes more significant. Many engineering applications of thermal contact resistance (TCR) are associated with low contact pressure with the presence of air (interstitial gas), therefore modeling the non-conforming rough contacts with the presence of interstitial gas is an important issue.

To the authors' knowledge there is no compact analytical model for predicting TCR of the non-conforming rough contacts with the presence of interstitial gas in the literature. The objective of this work is to develop a comprehensive, yet simple model for determining the heat transfer through the gap between non-conforming rough surfaces with the presence of an interstitial gas. A new approximate model is developed, which accounts for thermophysical properties of interstitial gas and solids, gas pressure, mechanical properties of solids, applied load, surface roughness, and surface curvature/out-of-flatness. The model covers the entire range of gas conduction heat transfer modes, i.e., continuum, slip, transition, and free molecular.

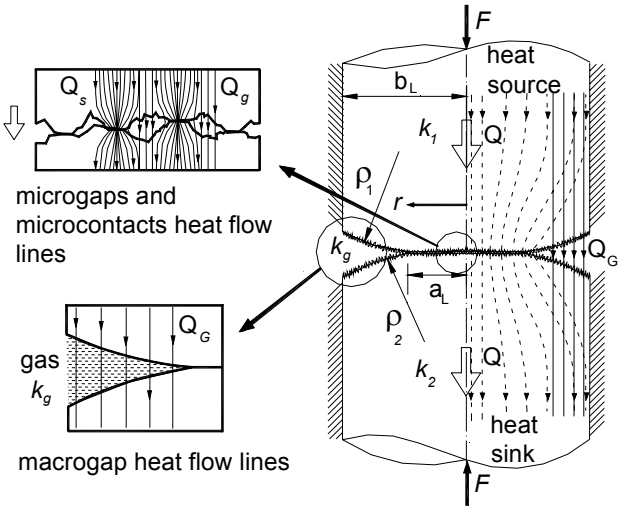

Fig. 1 Contact of non-conforming rough surfaces with presence of interstitial gas

Solid-Solid TCR

Bahrami et al.[2] studied mechanical contact of non-conforming rough surfaces. A closed set of governing relationships was reported for spherical rough contacts and solved numerically. The surface curvature was approximated by a truncated spherical profile.[3] Then the actual contact geometry of spheres was replaced by a flat surface and a profile, which resulted in the same undeformed gap between the surfaces.[4] Similar to Greenwood and Tripp,[5] the sphere profile was approximated by a parabola in the contact region. The bulk deformation was assumed to be within the elastic limit of the solids and the microcontacts were assumed to deform plastically. For convenience, all elastic deformations were considered to occur in one body, which had an effective elastic modulus and the other body was assumed to be rigid. The effective elastic modulus and the equivalent radius of curvature can be found from,

$$\begin{aligned} \frac{1}{\rho} &= \frac{1}{\rho_1} + \frac{1}{\rho_2} \\ \frac{1}{E'} &= \frac{1-\upsilon_1^2}{E_1} + \frac{1-\upsilon_2^2}{E_2} \end{aligned} \tag{1}$$

where subscripts 1 and 2 represents body 1 and 2 and E and υ are the elastic Young's modulus and the Poisson's ratio, respectively. As discussed in part one,[1] the contact between two Gaussian rough surfaces is

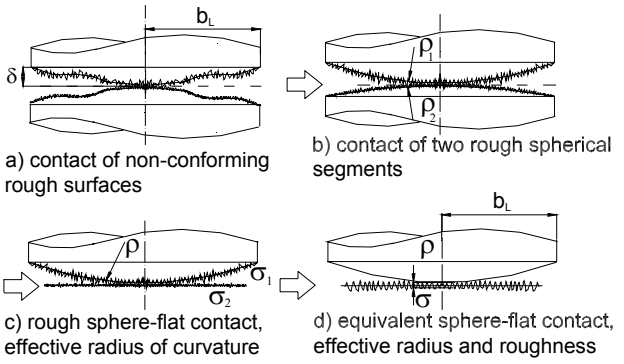

Fig. 2 Summary of geometrical modeling

modeled as the contact between a single Gaussian surface, having an effective surface characteristics, with a perfectly smooth surface, where the mean separation between two contacting planes, Y, remains the same. The equivalent roughness, σ, and surface slope, m, can be found from, $\sigma = \sqrt{\sigma_1^2 + \sigma_2^2}$ and $m = \sqrt{m_1^2 + m_2^2}$. Figure 2 summarizes the geometrical model. Clausing and Chao[3] used an approximate geometrical relationship to relate the surface radius of curvature ρ to the maximum surface out-of-flatness δ, i.e., $\rho = b_L^2/2\delta$. It should be noted that this relationship can be used for relatively large radii of curvature.

Bahrami et al.[2] proposed a general contact pressure distribution which covers the complete range of spherical rough contacts including the Hertzian smooth limit. Simple correlations developed for the maximum contact pressure, P_0, and radius of the macrocontact, a_L. Applying the Buckingham Π theorem, it was shown that there are two important governing non-dimensional parameters α and τ that describe the contact problem. The non-dimensional *roughness* parameter α, defined by Johnson,[4] is the ratio of roughness over the Hertzian maximum bulk deformation, $\omega_{0,H}$

$$\alpha = \frac{\sigma}{\omega_{0,H}} \equiv \frac{\sigma\rho}{a_H^2} = \sigma \left(\frac{16\rho E'^2}{9F^2} \right)^{1/3} \tag{2}$$

where $a_H = (0.75F\rho/E')^{1/3}$ is the Hertzian radius of contact, i.e., the limiting contact case where both surfaces are ideally smooth. The other non-dimensional parameter was chosen as,

$$\tau = \frac{\rho}{a_H} = \left(\frac{4E'\rho^2}{3F} \right)^{1/3} \tag{3}$$

The general pressure distribution[2] is

$$P(\xi) = P_0 \left(1 - \xi^2\right)^{\gamma} \tag{4}$$

$$P_0 = \frac{P_{0,H}}{1 + 1.37\alpha\ \tau^{-0.075}} \tag{5}$$

$$a_L = 1.80\ a_H\ \frac{\sqrt{\alpha + 0.31\tau^{0.056}}}{\tau^{0.028}} \tag{6}$$

where $P_{0,H} = 1.5F/\pi a_H^2$, $\xi = r/a_L$, and $\gamma = 1.5\,(P_0/P_{0,H})\,(a_L/a_H)^2 - 1$ are the maximum Hertzian contact pressure, dimensionless radial position, and the general pressure distribution exponent, respectively.

Bahrami et al.[6] using scale analysis methods developed an analytical model for determining the micro and the macro thermal resistances for contact of nonconforming rough surfaces in a vacuum. It was shown that the micro and macro thermal resistances are in series, i.e., $R_j = R_s + R_L$.

Assuming plastically deformed asperities, simple correlations were proposed[6] for predicting the microcontacts, R_s, and the macrocontact, R_L, thermal resistances in a vacuum,

$$R_s = \frac{0.57\,(\sigma/m)}{k_s F}\ c_1 \left(\frac{\sigma'}{m} \right)^{c_2} \tag{7}$$

$$R_L = \frac{(1 - a_L/b_L)^{3/2}}{2k_s a_L} \tag{8}$$

where,

$$k_s = \frac{2k_1 k_2}{k_1 + k_2}$$

where $\sigma' = \sigma/\sigma_0$ and $\sigma_0 = 1\ \mu m$, c_1, c_2, k_s, and F are a reference value, correlation coefficients determined from the Vickers microhardness measurements,[7] the harmonic mean of solid thermal conductivities, and the applied load, respectively.

Thermal Resistance of Interstitial Gas

Part one[1] of this work is dedicated to develop an approximate simple model for predicting the conduction heat transfer through the microgap between conforming rough surfaces. Conduction heat transfer in a gas layer between two parallel plates is commonly categorized into four heat-flow regimes;[8] continuum, temperature-jump or slip, transition, and free-molecular. The parameter that characterizes the regimes is the Knudsen number, $Kn = \Lambda/d$, where Λ and d are the molecular mean free path and the distance separating the two plates, respectively. The molecular mean free path is defined as the average distance a gas molecule travels before it collides with another gas molecule and it is proportional to the gas temperature and inversely proportional to the gas pressure[9]

$$\Lambda = \frac{P_0}{P_g}\frac{T_g}{T_0}\ \Lambda_0 \tag{9}$$

where Λ_0 is the mean free path value at some reference gas temperature and pressure T_0 and P_0.

Yovanovich[10] proposed that the heat transfer in a gas layer between two isothermal plates for all four flow regimes can be effectively calculated from

$$q_g = \frac{k_g}{d + M}\,(T_1 - T_2) \tag{10}$$

where T_1, T_2, d, k_g, and q_g are the uniform temperatures and the distance between the two isothermal parallel plates, gas thermal conductivity, and the gap heat flux, respectively. The gas parameter, M, is defined as:

$$M = \left(\frac{2-TAC_1}{TAC_1} + \frac{2-TAC_2}{TAC_2}\right)\left(\frac{2\gamma_g}{1+\gamma_g}\right)\frac{1}{\Pr}\,\Lambda \tag{11}$$

where TAC_1, TAC_2, γ_g, Pr, Λ are thermal accommodation coefficients corresponding to the gas-solid combination of plates 1 and 2, ratio of the gas specific heats, gas Prandtl number, and molecular mean free path at P_g and T_g, respectively.

In part one,[1] it was shown that the thermal joint resistance of conforming rough contacts can be considered as the parallel combination of the microcontacts and the interstitial gas thermal resistances, i.e., $R_{j,\text{flat}} = (1/R_s + 1/R_g)^{-1}$. As previously mentioned, due to the surface roughness the real contact area is a small portion of the apparent contact area, i.e., $A_r \ll A_a$. Assuming the microgap heat transfer area is equal to the apparent contact area, i.e., $A_g = A_a$; it was shown that for conforming rough contacts, $d = Y$, where Y is the separation between the mean planes of contacting surfaces. This simplified the microgap geometry, therefore the heat transfer through interstitial gap becomes equal to the heat transfer between two isothermal parallel plates located at the distance Y from each other, i.e.,

$$Q_g = \frac{k_g \Delta T}{M+Y} A_a \tag{12}$$

It was shown that[1]

$$\lambda = \frac{Y}{\sqrt{2}\sigma} = \text{erfc}^{-1}\left(\frac{2P}{H'}\right) \tag{13}$$

where $\text{erfc}^{-1}(\cdot)$, $H' = c_1 (1.62\sigma'/m)^{c_2}$, $P = F/A_a$, and A_a are the inverse complementary error function, the effective microhardness, contact nominal pressure, and the apparent macrocontact area, respectively.

The inverse complementary error function $\text{erfc}^{-1}(x)$ can be determined from[1]

$$\text{erfc}^{-1}(x) = \begin{cases} \dfrac{1}{0.218 + 0.735\ x^{0.173}} & 10^{-9} \le x \le 0.02 \\ \dfrac{1.05\,(0.175)^x}{x^{0.12}} & 0.02 < x \le 0.5 \\ \dfrac{1-x}{0.707 + 0.862x - 0.431x^2} & 0.5 < x \le 1.9 \end{cases} \tag{14}$$

The maximum relative difference between Eq. (14) and $\text{erfc}^{-1}(x)$ is less than 2.8 percent for the range of $10^{-9} \le x \le 1.9$.

The approximate model developed in part one[1] was compared with more than 510 experimental data points collected by Hegazy[7] and Song.[11] Tests were performed with SS 304 and nickel 200 with three gases, i.e., argon, helium and nitrogen. The data covered a wide range of surface characteristics, applied load, thermal and mechanical properties and the gas pressure, which was varied from vacuum to the atmospheric pressure. The model showed good agreement with the data over entire range of the comparison. The RMS relative difference between the model and data was determined to be approximately 10.9 percent.

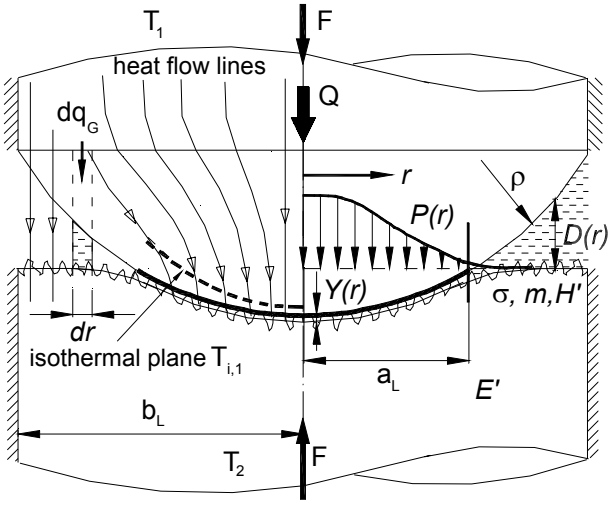

Fig. 3 Non-conforming rough contact heat transfer in gaseous environment

Present Model

The modeled geometry of the contact is shown in Fig. 3, the actual contact of two non-conforming rough surfaces is simplified to the contact of a flat rough, having the equivalent surface roughness σ, surface slope m, microhardness H', and the effective elastic modulus E', with a smooth rigid spherical profile which has the equivalent radius of curvature ρ. It is assumed that the contacting surfaces have Gaussian roughness and the asperities deform plastically; the bulk material deforms elastically. It is assumed that the contact planes are isothermal.

Total heat flow through the joint includes the heat transfer through:

- solids or microcontacts, Q_s
- the microgap within the macrocontact area, Q_g
- the macrogap between non-contacting parts of bodies, Q_G

TCR of non-conforming rough surfaces with the presence of interstitial gas contains four thermal resistance components, 1) the macrocontact constriction/spreading resistance, R_L, 2) the microcontacts constriction/spreading resistance, R_s, 3) resistance of interstitial gas in the microgap, R_g, and 4) thermal resistance of interstitial gas in the macrogap, R_G.

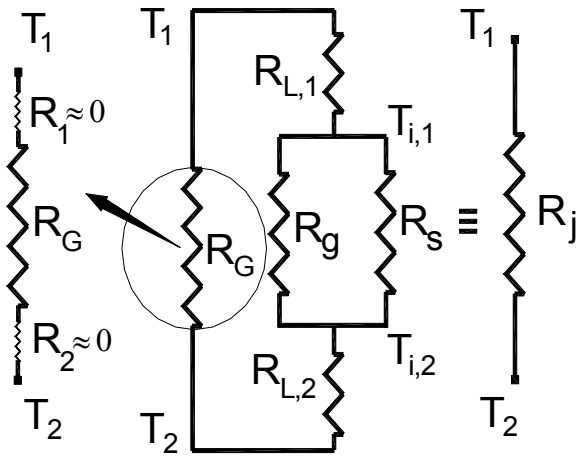

Fig. 4 Thermal resistance network, non-conforming rough contact

The effective microcontacts and the macrocontact thermal resistances, i.e., R_s and R_L can be determined using Eqs. (7) and (8), respectively.

Microcontacts can be modeled as isothermal heat sources on a half-space. Considering circular shape microcontacts with the radius a_s in the order of μm, isothermal planes with some intermediate temperatures $T_{i,1}$ and $T_{i,2}$ at depth l must exist in bodies one and two, respectively, see Fig. 3. For example in body one, it can be written, $T_1 < T_{i,1} < T_{c,1}$ where $T_{c,1}$ is the contact plane temperature. Under vacuum condition, the distance between the isothermal planes and the contact plane is $l = 40a_s \sim 40$ μm.[12] Macrocontact thermal constriction/spreading resistances $R_{L,1}$ and $R_{L,2}$ can be considered in series between the heat source, T_1, and the isothermal plane $T_{i,1}$ and the isothermal plane $T_{i,2}$ and the heat sink T_2, respectively. By increasing the gas pressure, heat flow through the microgap increases and the distance l decreases. The macrogap, the gap between the non-contacting area of the sphere and the flat, provides a parallel path for transferring heat from the heat source to the sink. Figure 4 represents the thermal resistance network for a non-conforming rough contact. Therefore, the thermal joint resistance can be written as

$$R_j = \left(\frac{1}{\left(1/R_s + 1/Rg\right)^{-1} + R_L} + \frac{1}{R_G} \right)^{-1} \qquad (15)$$

where $R_L = R_{L,1} + R_{L,2}$ is the macrocontact constriction/spreading thermal resistance.

The macrogap thermal resistance is considered to provide a parallel path between the heat source and the sink. As shown in Fig. 4, R_G has three components: the macrogap resistance and R_1 and R_2 corresponding to the bulk thermal resistance of the solid layers in body 1 and 2, respectively. Considering the fact that the gas thermal conductivity is much lower than solids, i.e., $k_g/k_s \leq 0.01$, the solid layers bulk resistances R_1 and R_2 compared to R_G are negligible.

Microgap Thermal Resistance, R_g

To determine the gas heat transfer through the microgap, the macrocontact area is divided into infinitesimal surface elements, dr, where the contact pressure can be assumed uniform. Therefore, the conforming rough microgap relationship Eq. (12) can be used for each surface element. By integrating the local heat flow through the interstitial gas in the microgap over the macrocontact area, we obtain

$$Q_g = \iint \frac{k_g \left(T_{i,1} - T_{i,2}\right)}{Y\left(r\right) + M} dA_g \qquad (16)$$

Note that the microgap resistance R_g accounts for the resistance between two isothermal planes at temperatures, $T_{i,1}$, and $T_{i,2}$, Fig. 3 see part one[1] for more detail. The macrocontact area is a circle with radius a_L; since $A_g = A_a - A_r$ and $A_r \ll A_a$, thus one can write $dA_g = dA_a = 2\pi r dr$. Using the definition of thermal resistance, i.e., $R_g = \left(T_{i,1} - T_{i,2}\right)/Q_g$ and Eq. (16), microgap thermal resistance can be written as,

$$R_g = \frac{1}{2\pi k_g} \left[\int_0^{a_L} \frac{r dr}{Y\left(r\right) + M} \right]^{-1} \qquad (17)$$

To determine R_g, the local plane separation, $Y\left(r\right)$, is required. The governing relationships and the numerical algorithm to calculate $Y\left(r\right)$ were explained in Bahrami et al.[2] To avoid a numerical solution, an approximate expression for the non-dimensional separation is developed by using the general pressure distribution correlation.

Due to surface curvature, the plane separation Y is not uniform throughout the macrocontact; it has its minimum at the center of the contact and increases as radial position, r, increases. Considering an infinitesimal surface element dr, where contact pressure can be considered uniform, the local non-dimensional plane separation using Eq. (13) is

$$\frac{2P\left(\xi\right)}{H'} = \text{erfc}\ \lambda\left(\xi\right) \qquad (18)$$

where $\lambda\left(\xi\right) = Y\left(\xi\right)/\sqrt{2}\sigma$, and $\xi = r/a_L$ are the non-dimensional plane separation, and the non-dimensional radial position, respectively.

The general pressure distribution satisfies the following conditions,

1. $dP\left(\xi\right)/d\xi = 0$, at $\xi = 0$, contact is axisymmetric
2. $P\left(\xi\right) = P_0$, at $\xi = 0$, the maximum contact pressure is known, i.e., Eq. (5)
3. $P\left(\xi\right)/P_0 \approx$ negligible, at $\xi = 1$, the contact pressure is negligible at $r = a_L$.

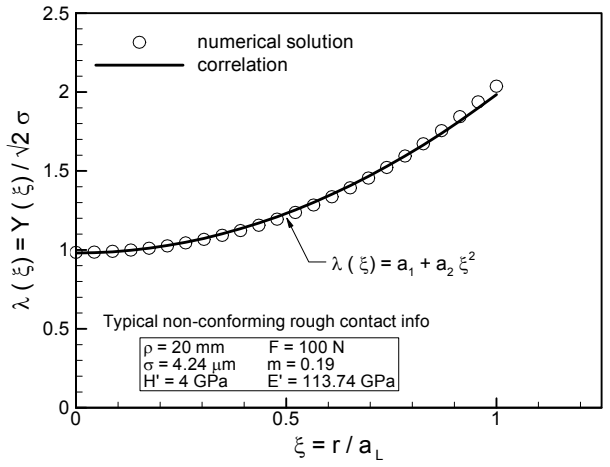

Fig. 5 Non-dimensional separation, non-conforming rough contact

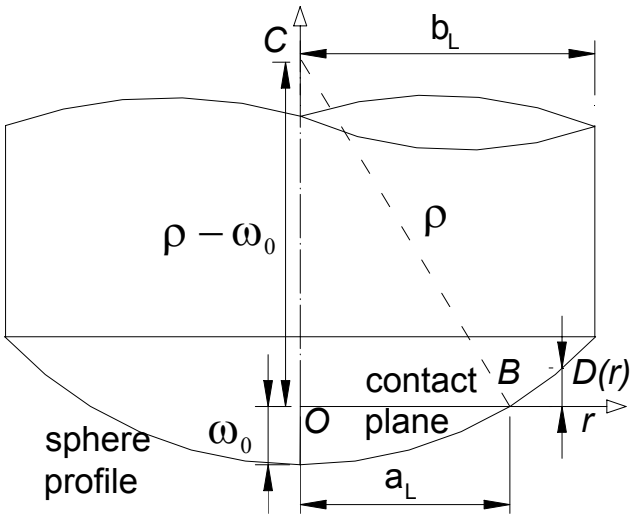

Fig. 6 Macrogap geometery

Assuming a parabolic shape for $\lambda(\xi)$ and using the above-mentioned conditions and Eq. (18), an expression for $\lambda(\xi)$ can be found as

$$\lambda(\xi) = a_1 + a_2\xi^2 \tag{19}$$

where,

$$a_1 = \text{erfc}^{-1}\left(\frac{2P_0}{H'}\right)$$
$$a_2 = \text{erfc}^{-1}\left(\frac{0.03P_0}{H'}\right) - a_1$$

where P_0 is given by Eq. (5). Equation (19) is compared with the numerical output of the computer program discussed in Bahrami et al.[2] in Fig. 5, for a typical contact. As shown, the agreement between Eq. (19) and the numerical results[2] is reasonable.

Substituting Eq. (19) into Eq. (17), after evaluating and simplifying the integral, R_g can be found from

$$R_g = \frac{\sqrt{2}\sigma a_2}{\pi k_g a_L^2 \ln\left(1 + \frac{a_2}{a_1 + M/\sqrt{2}\sigma}\right)} \tag{20}$$

In the conforming rough limit where surfaces are flat $\rho \to \infty$, $a_L \to b_L$, pressure distribution becomes uniform over the macrocontact area, i.e., $dP/dr = 0$, and $P = P_0 = F/\pi b_L^2$. Consequently, the mean separation, Y, will be uniform throughout the macrocontact area. Using the above-mentioned conditions for the general pressure distribution, $a_2 = 0$ and $a_1 = \text{erfc}^{-1}\left(2P/H'\right)$. Substituting these new values in Eq. (20) and using the L'Hopital's rule, one finds

$$\lim_{a_2 \to 0} R_g = \frac{Y + M}{k_g A_a}$$

which is the conforming microgap thermal resistance developed in part one of this study.[1] Note that for conforming rough contacts, $\text{erfc}^{-1}\left(2P/H'\right) = \lambda = Y/\sqrt{2}\sigma$.

Macrogap Thermal Resistance, R_G

Following the same method used to calculate the microgap thermal resistance, the macrogap area A_G, i.e., the non-contacting region of the solids is divided into infinitesimal surface elements dr. As discussed earlier, neglecting the bulk resistance of solid layers in bodies 1 and 2 compared with the macrogap resistance, heat transfer through interstitial gas, Q_G, can be determined using Eq. (12)

$$Q_G = \iint \frac{k_g(T_1 - T_2)}{D(r) + M} dA_G \tag{21}$$

where $D(r)$, T_1, and T_2 are the sphere profile in the non-contacting region, and the heat source and sink temperatures, respectively. Using thermal resistance definition, i.e., $R_G = (T_1 - T_2)/Q_G$, one obtains

$$R_G = \frac{1}{2\pi k_g}\left[\int_{a_L}^{b_L} \frac{r dr}{D(r) + M}\right]^{-1} \tag{22}$$

The macrogap profile of a sphere-flat contact with the radius ρ and the maximum deformation ω_0 is shown in Fig. 6. Even though the normal stress (contact pressure) is zero (negligible) beyond the macrocontact area, due to shear stress in the elastic half-space the normal deformation at the edge of the macrocontact is not zero. However in this study for convenience, that deformation is neglected, i.e., $\omega(r = a_L) = 0$. The maximum normal deformation ω_0 is much smaller than the radius of the sphere, $\omega_0 \ll \rho$, thus in the right triangle OCB, Fig. 6, one can write

$$\omega_0 = \frac{a_L^2}{2\rho} \tag{23}$$

Table 1 Input parameters for a typical SS-Nitrogen contact

$TAC_{SS-N_2} = 0.78$	$F = 100\ N$
$b_L = 12\ mm$	$\Lambda_0 = 6.25e-9\ m$
$\rho = 20\ mm$	$k_g = 0.026\ W/mK$
$P_g = 200\ torr$	$T_g = 300\ K$
$\sigma = 4.24\ \mu m$	$k_s = 10\ W/mK$
$m = 0.19$	$c_1,\ c_2 = 4\ GPa,\ 0$

Profile of the circle $D(r)$ with the radius ρ and the center coordinate $(0,\ \rho - \omega_0)$ is

$$D(r) = \rho - \omega_0 - \sqrt{\rho^2 - r^2} \tag{24}$$

where $a_L \leq r \leq b_L$.

Substituting Eq. (24) into Eq. (22), after evaluating and simplifying the integral

$$2\pi k_g R_G = \frac{1}{S \ln\left(\frac{S-B}{S-A}\right) + B - A} \tag{25}$$

where, $A = \sqrt{\rho^2 - a_L^2}$, $B = \sqrt{\rho^2 - b_L^2}$, and $S = \rho - \omega_0 + M$.

It can be seen that in the conforming limit where $\rho \to \infty$ consequently $a_L \to b_L$, the macrogap resistance $R_G \to \infty$.

Parametric Study

The effects of main input parameters on thermal joint resistance of a typical contact, indicated in Table 1, is investigated. Effects of external load F, surface roughness σ, gas pressure P_g, and surface radius of curvature ρ on the joint thermal resistance and its components are plotted in Figs. 7 to 10, respectively. The contacting surfaces are stainless steel and the interstitial gas is nitrogen at 300 K and 200 $torr$. Trends of the model are studied for a range of each input parameter, while the remaining parameters in Table 1 are held constant.

As illustrated in Fig. 7, in relatively small loads, due to small size and number of microcontacts, the microcontact resistance R_s is large, also the separation between two bodies is large, thus the microgap resistance R_g is high. At relatively light loads the macrocontact area is small, thus the macrocontact resistanceR_L is large. It can be seen that at relatively light loads, the joint resistance is close to the macrogap resistance, in other words most of the heat transfer take place through the interstitial gas in macrogap. By increasing the applied load, i) microcontacts resistance R_s decreases linearly, Eq. (7), ii) the separation between planes decreases which results in a decrease in the microgap resistance, R_g, iii) radius of the macrocontact a_L is increased which leads to a decrease in macrocontact resistance R_L, Eq. (8), and iv) the macrogap thermal resistance R_G increases (slightly).

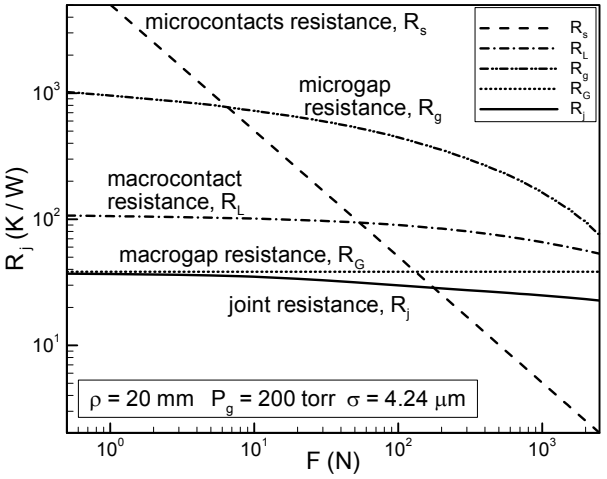

Fig. 7 Effect of load on thermal joint resistance

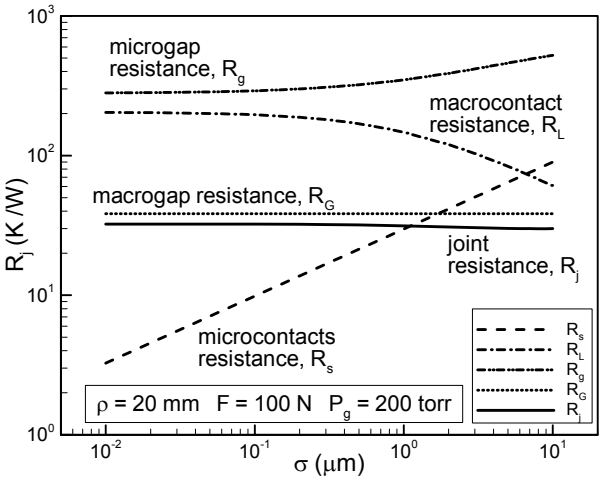

Fig. 8 Effect of roughness on thermal joint resistance

The joint resistance Eq. (15) decreases as external load increases.

The effect of surface roughness σ is shown in Fig. 8. As surface roughness is increased, while other contact parameters are kept constant, results in, i) the separation between two mean planes Y increases, thus the microgap resistance R_g increases, ii) the microcontacts resistance R_s increases linearly, Eq. (7), and iii) an increase the macrocontact area which leads to a lower macrocontact resistance R_L and higher (slightly in this case) macrogap resistance R_G. In total, increasing surface roughness results in a decreases in the joint resistance (for this contact).

The gas pressure is varied from vacuum to the atmospheric pressure and the joint resistance and its components are plotted in Fig. (9). The microcontacts R_s and the macrocontact R_L thermal resistances remain unchanged as the gas pressure varies. The macrogap R_G and the microgap R_g thermal resistances approach infinity for vacuum condition, thus the joint

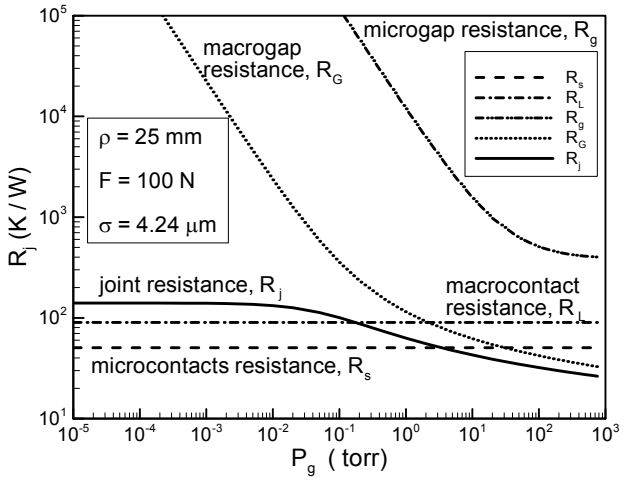

Fig. 9 Effect of gas pressure on thermal joint resistance

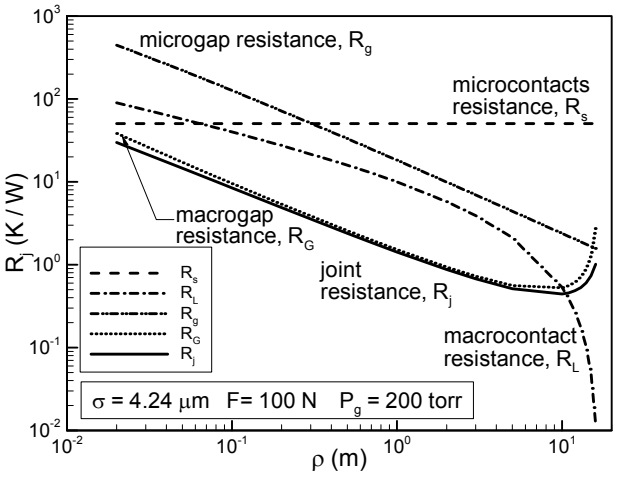

Fig. 10 Effect of radius of curvature on thermal joint resistance

resistance becomes simply the summation of the microcontacts R_s and macrocontact R_L resistances, Eq. (15). As the gas pressure increases, the gap resistances R_g and R_G drop, as a result the joint resistance decreases.

Figure 10 illustrates the effect of surface curvature on the joint resistance. As the radius of curvature increases, radius of the macrocontact increases, consequently the macrocontact resistance R_L decreases. An increase in radius of the macrocontact area, a_L, leads to a decrease in the microgap resistance R_g, see Eq. (20). The dependency of macrogap resistance R_G on the radius of curvature is complex, Eq. (25), increasing the radius of curvature, the macrogap resistance decreases up to a certain value of surface curvature, then in the limit where surfaces become flat $a_L \rightarrow b_L$, the macrogap resistance approaches infinity. It can be seen that for a fixed contact and gas pressure a surface curvature exists that minimizes the joint resistance. It also can be seen that the microcontacts resistance R_s is not a function of surface curvature, see Bahrami et al.[6] for more detail.

Comparison With Experimental Data

The present model is compared with more than 110 experimental data points collected by Kitscha.[13] The geometry of the experimental set up was as shown in Fig. 3. Two spherical carbon steel samples (radii 12.7 and 25.4 mm) and a steel-1020 flat specimen with surface roughness of $\sigma = 0.127\ \mu m$ were used. Specimens were cylindrical with the same radius, $b_L = 12.7\ mm$. Samples were placed in contact by applying external loads in a chamber filled with an interstitial gas. To minimize the radiation and convection heat transfer to the surroundings, lateral surfaces of specimens were insulated. The interstitial gases were air and argon, the gas pressure was varied from vacuum $\approx 10^{-5}$ to 700 *torr*. Table 2 summarizes the experiment numbers,

Table 2 Summary of Kitscha experiments

test	ρ	gas	F
	mm		N
T1	12.7	air	16.7 - 467
T2	25.4	air	16.9 - 135
T3	12.7	argon	17.8 - 467

Table 3 Properties of air and argon

gas	k_g	Pr	TAC	γ_g	Λ_0
	W/mK				nm
air	.0021+8E-5T	0.70	0.87	1.39	64.01
Ar	.0159+4E-6T	0.67	0.9	1.67	66.55

specimen radius of curvature, gas, range of applied load of the Kitscha's experimental data.

The mean contact temperature, i.e., the mean gas temperature was maintained at approximately 40 $^\circ C$; the harmonic mean thermal conductivities of the specimens was reported as 49 W/mK. Thermal properties of argon and air are listed in Table 3.[11,14] Note that the reference mean free paths, Λ_0, are at 288 K and 760 *torr* and temperature in k_g correlations must be in kelvin.

Tests were conducted at different external loads, at each load the gas pressure increased from vacuum approximately 10^{-5} to 700 *torr* while the load kept constant. Figure 11 illustrates the comparison between the present model and Kitscha[13] experimental data. For each data set, radius of curvature, load, and the interstitial gas are indicated, for example ρ12-F56Air means, radius of curvature was $\rho = 12.7\ mm$, applied load was $F = 56\ N$, and the interstitial gas was air. The horizontal axis is the thermal joint resistance predicted by the model, i.e. Eq. (15), and the vertical axis shows the experimental data. Therefore, the model is shown by the 45-degree line; also ±15 percent bounds of the model are included in the comparison.

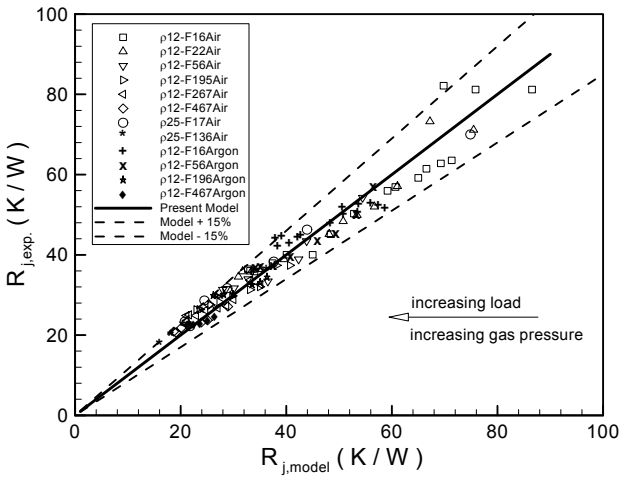

Fig. 11 Comparison of present model with Kitscha data

As shown in Fig. 11, the data shows good agreement with the model. The relative RMS difference between the model and the data is approximately 7.2 percent.

Concluding Remarks

An approximate analytical model was developed for determining TCR of non-conforming random rough contacts with the presence of an interstitial gas. Uniform temperatures for the contacting surfaces were assumed. Using general pressure distribution,[2] a relationship for local separation was developed. Employing this relationship in the conforming rough gap model developed in part one of this study,[1] a relationship for microgap thermal resistance of non-conforming rough contacts was derived.

Integrating local heat transfer over the non-contacting parts of contacting bodies, an expression for the macrogap resistance was found. The present model covers the four regimes of heat conduction modes of gas, i.e., continuum, temperature-jump or slip, transition, and free molecular and accounts for gas and solid mechanical and thermal properties, gas pressure and temperature, surface roughness, surface curvature, and the applied load.

Effects of main input parameters on the joint thermal resistances and its components predicted by the model were plotted and discussed. In particular, it was shown that for a rough sphere-flat contact at relatively light loads, most of the heat transfer take place through the interstitial gas in the macrogap. This represents the importance of the macrogap heat transfer, specially in light loads. The surface curvature has two competing effects on the joint resistance. It was observed that by increasing surface curvature the macrocontact and the macrogap and consequently the joint resistance decrease up to a certain value of surface curvature. As the surfaces approach the "flat surface" the macrocontact resistance approaches zero while the macrogap resistance approaches infinity. As a result of this trend, it was seen that a surface curvature exists that minimizes the joint resistance, while other contact parameters are kept constant.

The present model was compared with 110 experimental data points collected by Kitscha.[13] Tests were performed with carbon steel and steel-1020 with air and argon. The gas pressure was varied from vacuum to (almost) atmospheric pressure. The present model showed good agreement with the data over entire range of the comparison. The RMS relative difference between the model and data was determined to be approximately 7.3 percent.

References

[1]Bahrami, M., Culham, J. R., and Yovanovich, M. M., "Thermal Resistances of Gaseous Gap for Conforming Rough Contacts," *AIAA Paper No. 2004-0821, 42nd AIAA Aerospace Meeting and Exhibit, Jan 5-8, Reno, Nevada*, 2004.

[2]Bahrami, M., Culham, J. R., Yovanovich, M. M., and Schneider, G. E., "Thermal Contact Resistance of Non-Conforming Rough Surfaces Part 1: Mechanical Model," *AIAA Paper No. 2003-4197, 36th. AIAA Thermophysics Conference, June 23-26, Orlando, Florida*, 2003.

[3]Clausing, A. M. and Chao, B. T., "Thermal Contact Resistance in a Vacuum Environment," *Paper No.64-HT-16, Transactions of ASME: Journal of Heat Transfer*, Vol. 87, 1965, pp. 243–251.

[4]Johnson, K. L., *Contact Mechanics*, Cambridge University Press, Cambridge, UK., 1985.

[5]Greenwood, J. A. and Tripp, J. H., "The Elastic Contact of Rough Spheres," *Transactions of the ASME: Journal of Applied Mechanics*, Vol. 89, No. 1, 1967, pp. 153–159.

[6]Bahrami, M., Culham, J. R., and Yovanovich, M. M., "A Scale Analysis Approach to Thermal Contact Resistance," *Paper No. IMECE2003-44283, 2003 ASME International Mechanical Engineering Congress and RDD Expo, November. 16-21, Washington D.C.*, 2003.

[7]Hegazy, A. A., *Thermal Joint Conductance of Conforming Rough Surfaces: Effect of Surface Micro-Hardness Variation*, Ph.D. thesis, University of Waterloo, Dept. of Mech. Eng., Waterloo, Canada, 1985.

[8]Springer, G. S., "Heat Transfer in Rarefied Gases," *Advances in Heat Transfer, Edited by Irvine T. F. and Hartnett J. P.*, Vol. 7, 1971, pp. 163–218.

[9]Kenard, E. H., *Kinetic Theory of Gases*, McGraw-Hill, New York, London, 1938.

[10]Yovanovich, M. M., "Thermal Contact Correlations," *Progress in Aeronautics and Aerodynamics: Spacecraft Radiative Transfer and Temperature Control, in Horton, T.E. (editor)*, Vol. 83, 1982, pp. 83–95.

[11]Song, S., *Analytical and Experimental Study of Heat Transfer Through Gas Layers of Contact Interfaces*, Ph.D. thesis, University of Waterloo, Dept. of Mech. Eng., Waterloo, Canada, 1988.

[12]Bejan, A. and Kraus, D., *Heat Transfer Handbook*, John Willey, New York, 2003.

[13]Kitscha, W., *Thermal Resistance of the Sphere-Flat Contact*, Master's thesis, University of Waterloo, Dept. of Mech. Eng., Waterloo, Canada, 1982.

[14]Incropera, F. P. and Dewitt, D. P., *Fundamentals of Heat and Mass Transfer*, John Wiley, New York, 1996.